Journal of Instrumentation

Development of a novel wide-angle gamma-ray imaging air Cherenkov telescope with SiPM-based camera for the TAIGA hybrid installation

To cite this article: D. Chernov *et al* 2020 *JINST* **15** C09062

PUBLISHED BY IOP PUBLISHING FOR SISSA MEDIALAB

RECEIVED: *May 15, 2020*
ACCEPTED: *June 11, 2020*
PUBLISHED: *September 28, 2020*

INTERNATIONAL CONFERENCE ON INSTRUMENTATION FOR COLLIDING BEAM PHYSICS
NOVOSIBIRSK, RUSSIA
24–28 FEBRUARY, 2020

Development of a novel wide-angle gamma-ray imaging air Cherenkov telescope with SiPM-based camera for the TAIGA hybrid installation

D. Chernov,[a,1] I. Astapov,[b] P. Bezyazeekov,[c] E. Bonvech,[a] A. Borodin,[d] M. Brueckner,[e] N. Budnev,[c] D.Chernukh,[c] A. Chiavassa,[f] A. Dyachok,[c] O. Fedorov,[c] A. Gafarov,[c] A. Garmash,[g,h] V. Grebenyuk,[d,i] O. Gress,[c] T. Gress,[c] O. Grishin,[c] A. Grinyuk,[d] D. Horns,[j] A. Ivanova,[c,g] N. Kalmykov,[a] Y. Kazarina,[c] V. Kindin,[b] S. Kiryuhin,[c] R. Kokoulin,[b] K. Kompaniets,[b] E. Korosteleva,[a] V. Kozhin,[a] E. Kravchenko,[g,h] A.Krykov,[a] L. Kuzmichev,[a] A. Lagutin,[k] Yu. Lemeshev,[c] B. Lubsandorzhiev,[l] N. Lubsandorzhiev,[a] R. Mirgazov,[c] R. Mirzoyan,[c,m] R. Monkhoev,[c] E. Osipova,[a] A. Pakhorukov,[c] A. Pan,[d] M. Panasyuk,[a] L. Pankov,[c] A. Petrukhin,[b] D. Podgrudkov,[a,n] V. Poleschuk,[c] M. Popescu,[o] E. Popova,[a] A. Porelli,[e] E. Postnikov,[a] V. Prosin,[a] V. Ptuskin,[p] A. Pushnin,[c] R. Raikin,[k] G. Rubtsov,[l] E. Rybov,[c] Y. Sagan,[d,i] V. Samoliga,[a] A. Silaev,[a] A. Silaev (jr.),[a] A. Sidorenkov,[l] A. Skurikhin,[a] V. Slunecka,[d] A. Sokolov,[g,h] Y. Suvorkin,[c] L. Sveshnikova,[a] V. Tabolenko,[c] A. Tanaev,[c] B. Tarashansky,[c] L. Ternovoy,[c] L. Tkachev,[d,i] M. Tluczykont,[j] N. Ushakov,[l] A. Vaidyanathan,[g] P. Volchugov,[a,n] D. Voronin,[l] V. Vorobiov,[g,h] R. Wischnewski,[e] I. Yashin,[b] A. Zagorodnikov[c] and D. Zhurov[c]

[a] *Skobeltsyn Institute of Nuclear Physics MSU, Moscow, Russia*
[b] *NRNU MEPhI (Moscow Engineering Physics Institute), Moscow, Russia*
[c] *Institute of Applied Physics ISU, Irkutsk, Russia*
[d] *JINR, Dubna, Russia*
[e] *DESY, Zeuthen, Germany*
[f] *Dipartimento di Fisica Generale, Università di Torino and INFN, Torino, Italy*

[1] Corresponding author.

2020 JINST 15 C09062

 https://doi.org/10.1088/1748-0221/15/09/C09062

[g] *Novosibirsk State University, NSU,*
Novosibirsk, Russia
[h] *Budker Institute of Nuclear Physics SB RAS,*
Novosibirsk, Russia
[i] *Dubna State University,*
Dubna, Russia
[j] *Institut für Experimentalphysik, University of Hamburg,*
Hamburg, Germany
[k] *Altai State University,*
Barnaul, Russia
[l] *Institute for Nuclear Research of RAN,*
Moscow, Russia
[m] *Max-Planck-Institute for Physics,*
Munich, Germany
[n] *Lomonosov Moscow State University, Faculty of Physics,*
Moscow, Russia
[o] *ISS,*
Bucharest, Romania
[p] *IZMIRAN,*
Moscow, Russia

E-mail: chr@dec1.sinp.msu.ru

Abstract: The TAIGA complex-detector is designed to study gamma and cosmic rays in the energy range above 30 TeV. We are developing a novel wide-angle imaging air Cherenkov telescope with a SiPM based camera with a field of view of 15–20° and an aperture of around 1 m^2. In this report we present the design of the telescope imaging camera (optical and data acquisition systems), based on 1000–1200 SiPMs. The prototype of such camera, based on 49 SiPMs, is operating at the TAIGA's site in the Tunka valley since September 2019. The design of the prototype and the preliminary results of data analysis is presented.

Keywords: Cherenkov detectors; Gamma telescopes; Photon detectors for UV, visible and IR photons (solid-state) (PIN diodes, APDs, Si-PMTs, G-APDs, CCDs, EBCCDs, EMCCDs, CMOS imagers, etc)

2020 JINST 15 C09062

Contents

1 Introduction

Gamma-ray astronomy at energies above 30 TeV (very high energy (VHE) gamma-ray astronomy) still has a number of fundamental questions that yet are not answered and above all stands the question of the probable galactic sources of cosmic rays in the energy region of 1 PeV — the region immediately adjacent to the classical "knee" in the energy spectrum of primary cosmic rays (PCR). To the present day the bulk of knowledge about the fluxes and sources of very high energy gamma-rays had been obtained using imaging air Cherenkov telescopes (IACT).

An IACT usually consists of a set of (usually spherical shape) mirrors and a camera in which the image of a flash of Cherenkov light from extensive air showers (EAS), initiated by primary gamma and cosmic rays, is formed and recorded. The sensitivity level of existing and currently operational VHE gamma-ray telescopes is optimized for the 0.05–50 TeV energy range [1–4].

A modern existing IACT for this energy range is a complex and expensive engineering product. A serious drawback of a high-energy IACT is the small diameter of its field of view (FOV), which is typically no more than 5° [1–3] (the planned Small Size Telescope and Medium Size Telescope of the Cherenkov Telescope Array project will have a larger FOV [4, 5]). Such small FOV limits the observations to only a handful of sources during a single observation.

At present the first phase of deployment of the TAIGA installation [6, 7] is being finished in the Tunka Valley (Republic Buryatia, Russian Federation). The main goal of this experiment [7] is to study gamma rays at energies above 30 TeV. The installation is planned to have an array of wide-angle (0.6 sr) optical stations located on an area of 1 km^2 (TAIGA-HiSCORE array [8]) and 3 IACTs (TAIGA-IACT).

According to the TAIGA-HiSCORE data [8, 9] the direction and energy of EAS initiated both by gamma and charged cosmic rays can be reconstructed with high accuracy. For the analysis and separation of gamma-induced EASs from the PCR nuclei-induced EASs the image data from the TAIGA-IACT is combined with that from the TAIGA-HiSCORE array. Such a hybrid approach is effective for the selection of events induced by gamma rays even with large impact parameters.

To study the gamma rays above 30 TeV we propose to use a new wide-angle IACT with a FOV of 15° and an effective area of around 1 m^2, which will allow to observe multiple sources during a single night. A Fresnel lens is planned as the main element of the optical system of the telescope. In the future, an effort will be made to increase the FOV diameter up to 60 degrees making it comparable with the aperture of the TAIGA-HiSCORE.

2 SiPMs for high energy gamma-ray astronomy

Nowadays most of the IACTs use cameras based on vacuum photomultiplier tubes (PMT) [1–3]. This situation may change, especially for telescopes of small apertures and small plate-scales and SiPMs could be used as light sensors in the imaging cameras [10].

Cameras based on SiPMs have several advantages. First, SiPMs do not degrade under strong ambient light. Second, unlike PMTs the SiPMs have less sample-to-sample variations, they require an operational voltage of only a few tens of volts, are compact, light-weight and have low power consumption.

The first full-scale detector to use SiPMs was the First G-APD Cherenkov Telescope (FACT) [12]. In small size telescopes of the CTA project [5] a SiPM based imaging camera was developed [13, 14].

Another example is the ASTRI telescope that used Schwarzschild-Couder dual-mirror optics [16]. This led to a smaller geometric size of the camera and allowed to use only 4 standard 3×3 mm^2 SiPMs in one pixel. ASTRI was able to detect the Crab Nebula [17].

The LHAASO detector is planned to include 16 wide-angle telescopes (viewing angle 16×14°) based on specially designed new SiPM. This new SiPM is designed with 360 000 cells to make sure that it should not be saturated by at least 32 000 photoelectrons appearing simultaneously [18, 19].

The design, calibration procedures and long-term tests of SiPM-based pixels for large size Cherenkov telescopes are discussed in detail in [20].

A description of small size Cherenkov SiPM-based telescopes is given in [21, 22]. Both telescopes use Fresnel lens optics.

3 Wide-angle camera with silicon photomultipliers

For the analysis and separation of gamma-induced EAS from those by PCR nuclei the image data from TAIGA-IACT is combined with that coming from the TAIGA-HiSCORE array. Such hybrid approach is an effective means for gamma-nuclei separation. A significant difference between the apertures of the ground stations of the TAIGA-HiSCORE array and the Cherenkov telescopes of the TAIGA-IACT is a drawback of the existing installation. With a camera FOV of 9.6°, the solid angle of IACT is 25 times smaller than that of the TAIGA-HiSCORE stations [8] and, accordingly, only 4% of the events detected by the ground stations fall into the IACT's FOV.

In order to correct this drawback, as was mentioned above, presently a new IACT is designed with a 15° maximum viewing angle and effective area of around 1 m^2. The energy threshold of

2020 JINST 15 C09062

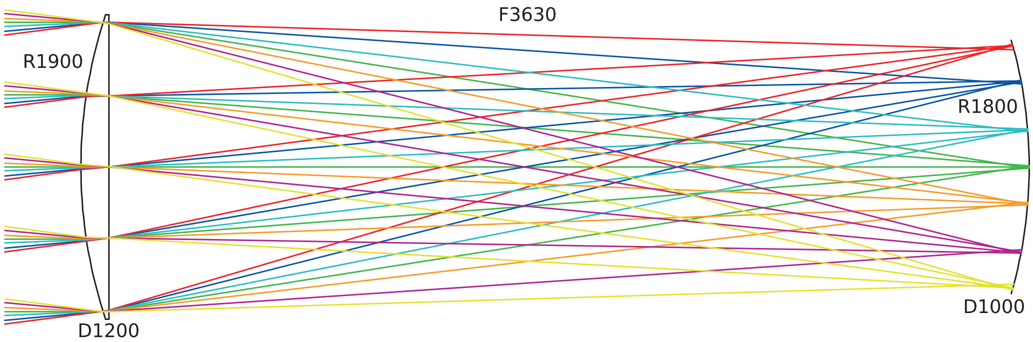

Figure 1. Preliminary version of the optical system for an ordinary lens (all dimensions in mm, see text for details).

such IACT will be approximately 10 TeV. The number of hybrid IACT-TAIGA-HiSCORE events in turn should increase by 3–4 times.

3.1 Scheme of the optical system

The new detector utilizes around 1000–1200 SiPMs for its imaging camera. The optical system of the new IACT is designed around a Fresnel lens.

One of the preliminary optical system designs with a 15° full viewing angle is shown in figure 1 (ray-tracing were performed using the OSLO program [23]). This version uses a simple plano-convex lens. The optical properties and dimensions of this version are a the starting point for the more complex designs with a Fresnel lens. The use of the Fresnel lens should significantly decrease the mass and size of the system with some increase in the optical resolution.

The lens diameter (see figure 1) is 1200 mm with 1900 mm curvature radius. Maximum thickness of this design is 110 mm (in the center). All calculations are performed for the CO-120A UV-absorption-reduced PMMA plastic. The actual lens (Fresnel or not) will be built from this material or its close analog. The diaphragm (not shown) will limit the system's entry window to 1140 mm in diameter. The focal distance for this preliminary lens is 3630 mm. The image is formed on the concave photon detection surface (PDS) with a 1000 mm diameter and 1800 mm curvature radius. The shape of the PDS has not been finalized yet. Both a flat surface and a spherical surface with a radius of about 2 m are still being discussed. The following preliminary results are shown for a spherical PDS.

The detailed images of light spots produced by parallel beams at the PDS are shown in figure 2. Different colors show results for light of different wavelengths: blue curve stands for 350 nm, green — 420 nm, red — 550 nm. The spots are shown for different incidence angles (0°, 5.27° and 7.5°) and different offsets of the PDS (±10 mm and ±20 mm).

The plots in figure 3 show the relative amount of light collected within a certain radius in the spot on the PDS for two incidence angles (0° and 7.5°). Here, same as above, different colors are used for different wavelengths (blue — 350 nm, green — 420 nm, red — 550 nm).

The light reaching the entrance of the PDS is focused onto the SiPMs by hollow light concentrators covering the full area of the PDS. The geometry of the concentrators has been optimized to reach the required 15° cut-of-angle. Seven light concentrators are structurally combined into a one

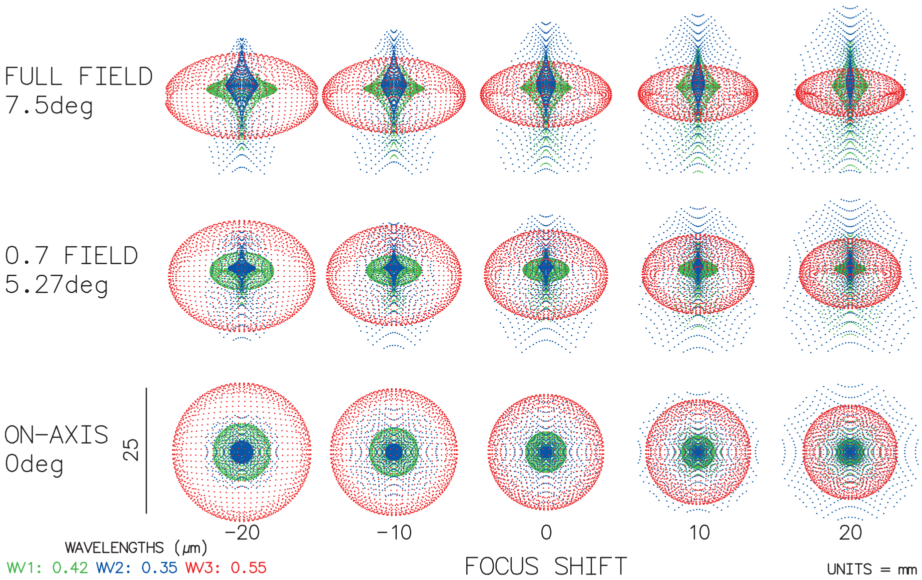

Figure 2. Spot diagram analysis. Colors for wavelengths: blue — 350 nm, green — 420 nm, red — 550 nm.

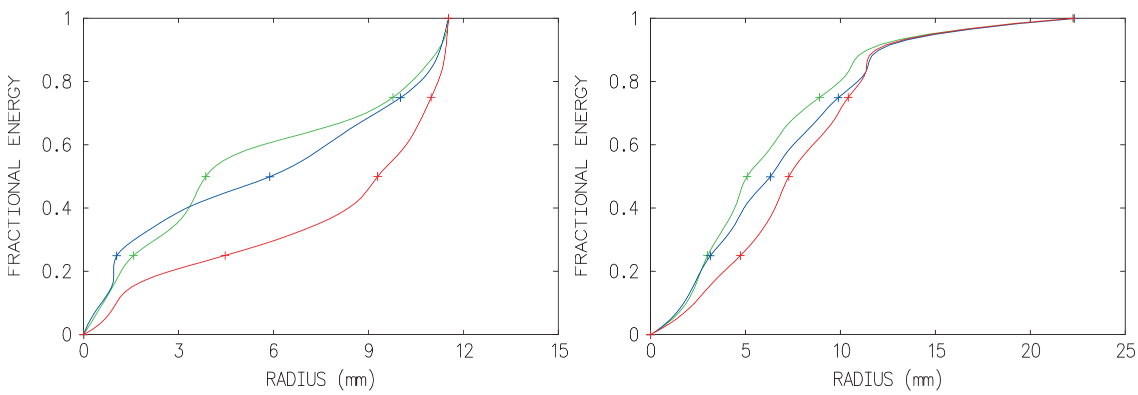

Figure 3. Spot radial energy distribution. From left to right shows distributions for light incidence angles 0° and 7.5°, where colors for wavelengths: blue — 350 nm, green — 420 nm, red — 550 nm.

light concentrator module (LCM) (see figure 4). Behind the LCM a 7-channel photon detection module (PDM) based on 7 SiPMs (not shown on the figure) is located.

The PDM has a mezzanine design consisting of a sensor board (SB) with 7 SiPMs and an interface board (IB). The distance between the SB and the IB will be only about 6 mm. The side of the IB facing the SB will be covered by grounded shielding, therefore, significantly decreasing the interference currents on the analog circuits of the SB as well as the mutual influence of analog circuits on each other.

Amplifiers are located on the IB on the opposite side from the SB. The IB transmits analog signals from SB to the data acquisition system (DAQ) controller board, and houses all necessary low-current low-noise devices such as digital-to-analog converters (DAC) for generating individual SiPM supply voltages, and etc. The IB is connected to the DAQ controller board using a flexible cable. In total up to 4 PDMs (28 pixels) can be connected to each DAQ controller board.

2020 JINST 15 C09062

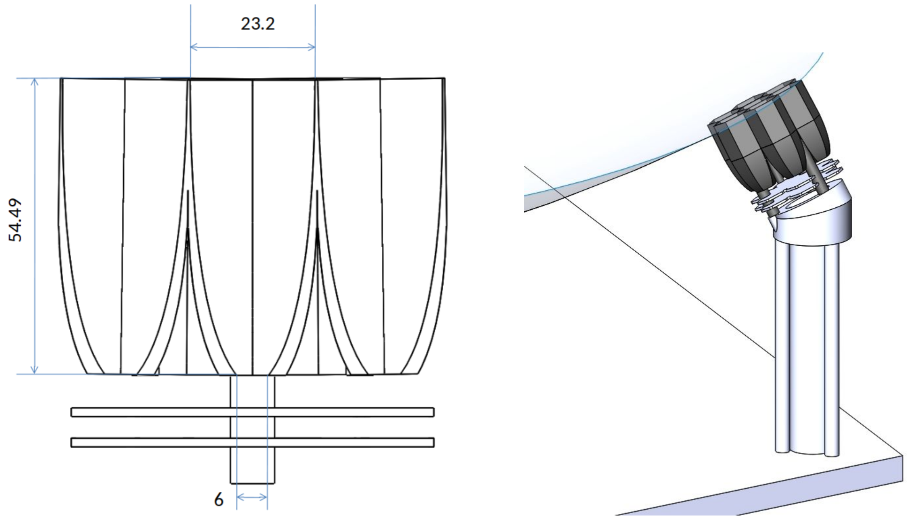

Figure 4. Cone light concentrators with PDM based on 7 SiPM sensors (left) and a 3D-model of the cone with holder (right).

3.2 Front end electronics and DAQ

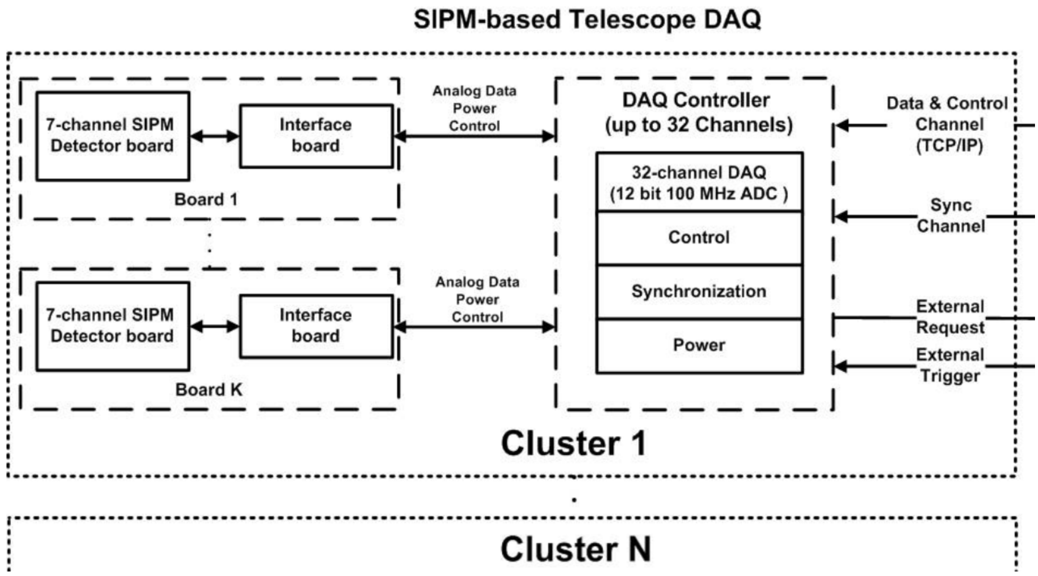

Figure 5. Preliminary version of the data acquisition system's cluster.

The PDMs produce analog signals that are amplified and routed to the DAQ controller board. There the analog signals are digitized and then processed by the FPGA in real time.

The DAQ controller board (see figure 5) is based on the Xilinx FPGA of the Zynq family [24] and four 8-channel 10-bit 100 MHz (or 12-bit 80 MHz) ADCs with a total of 32 channels.

The DAQ system logically represents a modular design, where each module consists of a DAQ controller board and 4 PDMs. Each DAQ controller board has a separate data and control channel (Ethernet, data transfer rate up to 600 Mbit/s) and a separate optical synchro-channel, through which

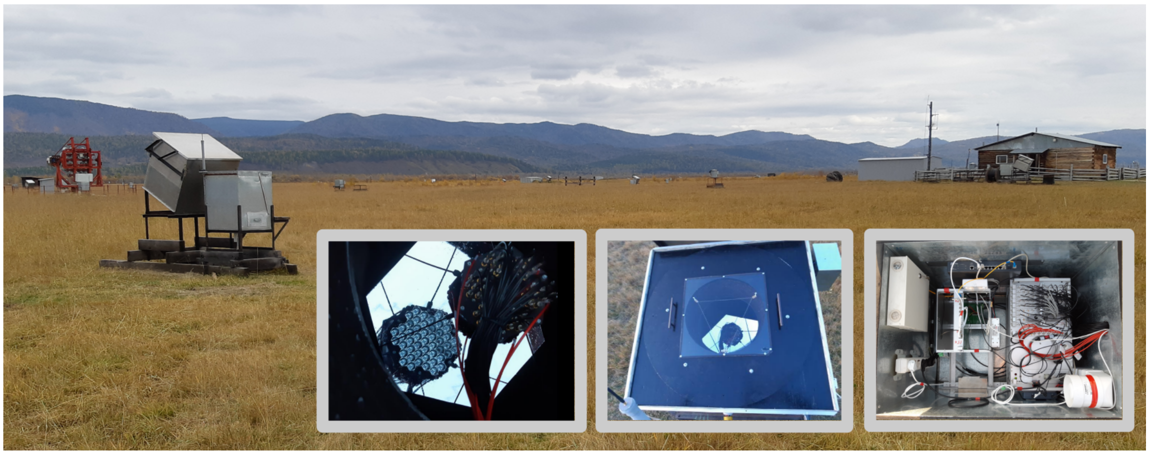

Figure 6. The photo shows from left to right: the prototype of the small image telescope (at a distance of ~100 m from the TAIGA-IACT), the 49-SiPM mosaic with mirror, the entrance window of the telescope with an open lid, and the measuring electronics in the thermo-stabilized box.

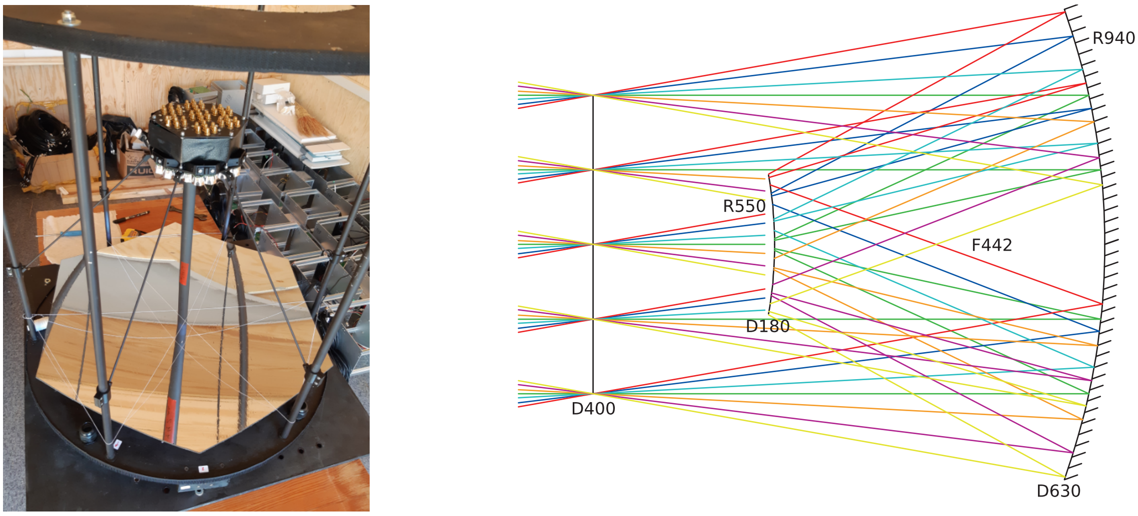

Figure 7. Alignment of the optical system (left). Scheme of the prototype's optical system (right).

it receives the clock frequency and synchronization time stamps. Accordingly, each DAQ controller board is integrated into the TAIGA common synchronization system [8].

For implementation of the global trigger for the entire camera, the DAQ controller board provides an "External Request" output for a signal from this board's local trigger condition to the external trigger board, and an "External Trigger" input for the global trigger signal from a separate trigger board. The global trigger is formed if a certain number of adjacent pixels of different PDMs on different DAQ controller boards are triggered ("topological condition"), thus seaming the PDMs into a uniform trigger matrix. Using these topological conditions the counting rate of the camera caused by random coincidences is decreased by several times.

The DAQ controller also provides power to the PDMs and collects telemetry data such as PDMs' temperatures, direct SiPM currents, and etc.

2020 JINST 15 C09062

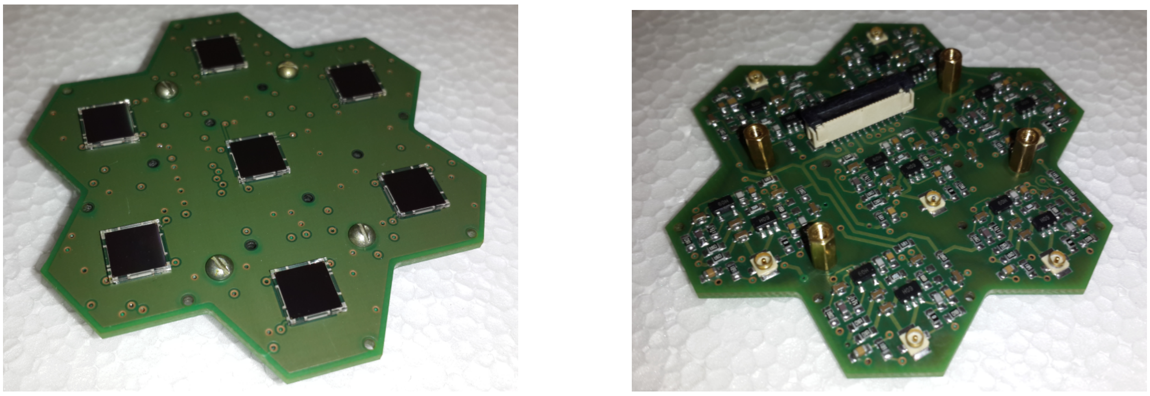

Figure 8. Prototype 7-segments SiPM electronic board (top and bottom views).

4 SIT prototype

For long-term testing of SiPMs and the measurement system, a small imaging telescope (SIT) based on 49 MicroFC-SMTPA-60035 SiPMs was installed in the Tunka Valley for joint operation with the TAIGA-HiSCORE array (see figure 6). The telescope uses the Schmidt optical system with a $\pm 8^{\circ}$ FOV and a 0.1 m^2 entrance window. The SIT is installed in a standard optical container of the TAIGA-HiSCORE station [8] and connected to the DAQ and synchronization system of this array. Photo of the assembly and alignment of the prototype, as well as the main parameters of the optical system are shown in figure 7.

The MicroFC-SMTPA-60035 SiPM used in SIT has a fast output and a 6×6mm^2 sensitive area. The camera matrix is assembled of 7-segments SiPM boards (photo in figure 8) with 7 SiPMs on each one. The fast output of each SiPM is connected to a two-stage preamplifier. The first stage works as a current to voltage amplifier-converter. The second stage is used to transmit the signal through a 50Ω micro-coaxial cable to the DAQ system. The FWHM of a single photoelectron pulse is about 20 ns and the amplitude at maximum SiPM gain ($5{\cdot}10^6$) is about 30 mV. A temperature sensor is installed on each SiPM board. Each SiPM power supply line has an ADC-DAC pair for constant monitoring and control of each SiPM gain.

The output of each SiPM is digitized by 80 MHz FADCs (the same was used before in the SPHERE-2 detector [25, 26]). After each trigger the DAQ system records 8.8 μs of data with approximately 0.7 μs of data before the trigger. Two modes for camera trigger generation are used: the signals in 3 adjacent pixels exceed the preset relatively low thresholds or a signal in any pixel exceeds a relatively high threshold.

To link the SIT events with those of TAIGA-HiSCORE the camera trigger generation time is measured also by the HiSCORE timer. The timer is synchronized through an optical fiber with the synchronization module of the HiSCORE array. The SIT trigger signal is transferred via a cable to the HiSCORE timer where its arrival time is measured and stored with a certain number. That number in a serial code is transmitted from the timer via the RS-485 output back to the FADC analog input. The digitized signal from the output of this channel is transmitted together with the data from all channels to the DAQ system where it is digitized along with the event. The figure 9 shows an example of an event waveform from all 49 SiPMs (colored curves) and a synchronization

2020 JINST 15 C09062

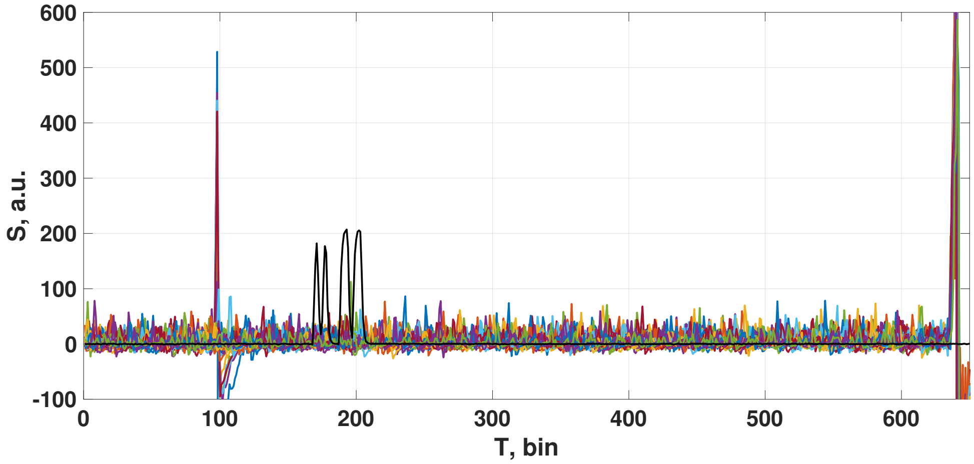

Figure 9. An example of a full length oscillogram for an event.

channel (black curve) connected to the HiSCORE timer. The signal from the EAS is located near the 100$^{\text{th}}$ time bin. The HiSCORE timer code in serial binary code is written near the 200$^{\text{th}}$ time bin. At the end of the event the signals from flashes of the internal LED synchronisation system can be seen. These flashes are used for more accurate signal timing and data buffer shift control.

Using the TAIGA-HiSCORE array data and its timer stamps, the core location, arrival direction and primary energy of the EAS, which triggered the SIT, can be accessed and used for both SIT data analysis and SIT performance evaluation in different conditions.

5 Preliminary results of the SIT prototype

During the measurement period from September 2019 to January 2020 (in total over 220 hours of observations) more than 650 000 events were recorded. The average detector counting rate was near 1 Hz. The recorded event data along with the telemetry data was processed in order to identify the EAS events among all recorded events and to estimate their parameters.

The recorded signals in a single event (see figure 9) show some peaks corresponding to photo-electrons originating from night sky background light and electrons from the SiPM dark current. The peaks form the whole record in each channel, and not just near the trigger window, were analyzed. The spectrum of charges under these peaks for different SiPMs is shown in figure 10. The events in this spectrum were recorded at a temperature of 3°C and 28.65 V voltage on the SiPM. The spectrum clearly shows an asymmetrical distribution with an electronics noise peak near zero (fluctuations of the baseline), a single electron peak near 12 a.u., two-electrons peak at 25 a.u., and etc. The asymmetrical left part of the distribution comes from the relatively long afterpulses (see figure 15). A set of such curves was used to estimate the calibration coefficients for a given voltage and temperature.

The temperature of the SiPM camera was monitored constantly. The recorded temperature profiles during measurements for several days in January 2020 are presented in figure 11 (up). The profiles appear to be smooth as expected and are consistent with the meteorological data. But the SiPM camera temperatures are consistently higher than those of the outside air since the detector was in a weather protected box.

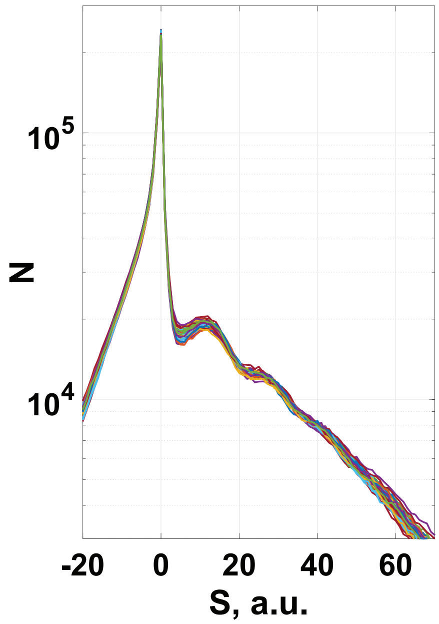

Figure 10. An example of the measured SiPM signals' amplitude spectra at $T = 3°C$ and $U = 28.65$ V. Different line colors correspond to different SiPMs.

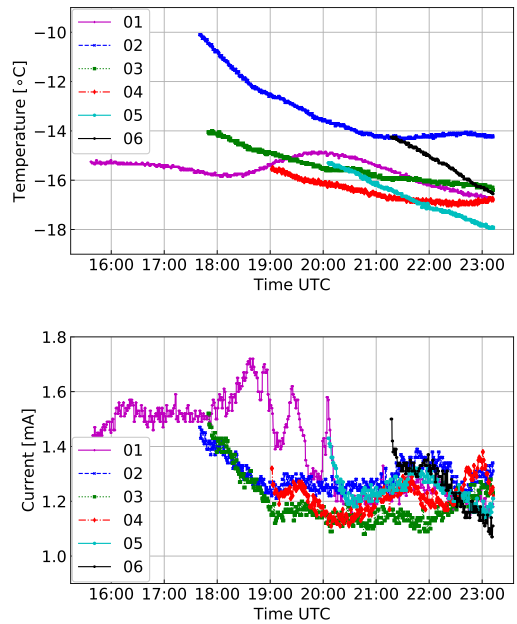

Figure 11. The SiPM mosaic temperature (up) and the SiPM total current (bottom) telemetry data for several days in January 2020.

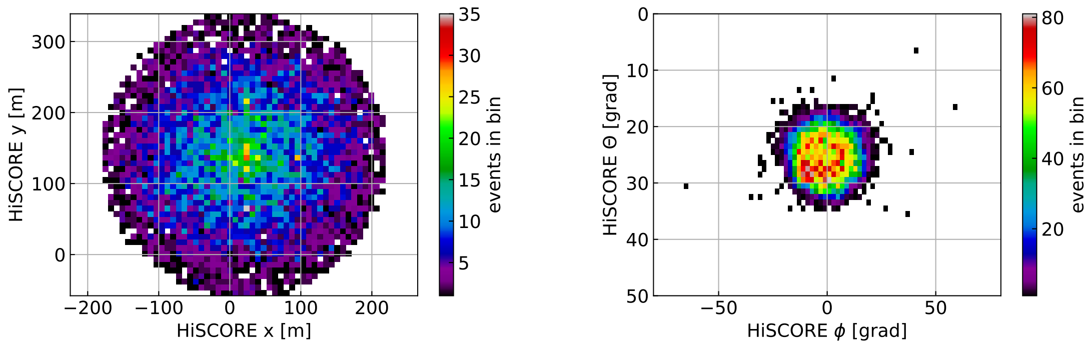

Figure 12. (On the left) The cores distribution of joint events across the HiSCORE detector (only the events within 200 m from SIT are shown). (On the right) The distribution of arrival directions for the joint events. The few single events far off the SIT FOV are due to random coincidences within a given trigger mark window.

The total SiPM current was monitored during measurements. The current value depends on the ambient light, SiPM temperature, voltage etc. The figure 11 (bottom) shows the SiPMs' current over several days in January 2020. The voltage on the SiPMs was the same over these days so the difference in SiPM currents in the beginning of the measurements hours can be explained by the night-to-night temperature variation and by the residual scattered moonlight. The high currents on January 1^{st} are due to the thin haze in the fist half of the night.

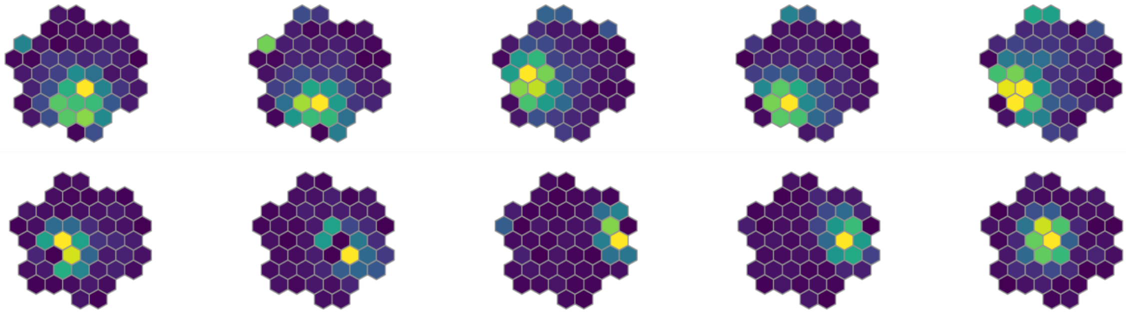

Figure 13. Examples of events recorded by the SIT prototype.

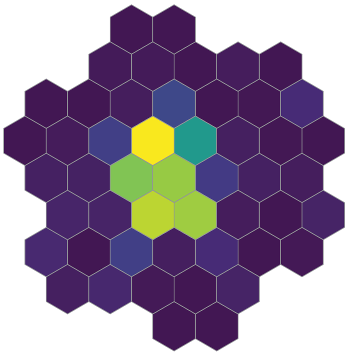

Figure 14. The SIT-536027 joint event image. Max amplitude is around 45 photoelectrons.

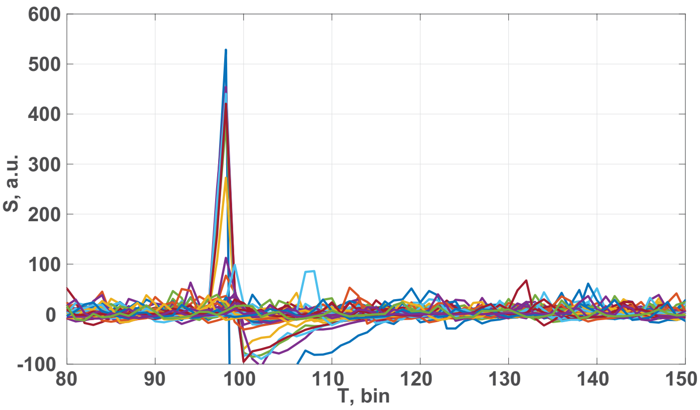

Figure 15. The oscillogram of the SIT-536027 event. Colors represent different channels. The photoelectrons produced a peak near the time bin 98.

As was mentioned above, the SIT prototype was synchronized with the TAIGA-HiSCORE array. Between 24.12.2019 and 06.01.2020 the SIT prototype and the TAIGA-HiSCORE array detected 14 517 joint events. The EAS arrival directions and core locations were derived from the TAIGA-HiSCORE data set analysis. The cors distribution for join events in the 200 m area from the SIT detector is presented in figure 12 (left). The bright point at (30;140) corresponds to the SIT detector location.

The SIT prototype has a viewing angle of ±10°. The majority of arrival directions for detected joint events is concentrated in the vicinity of the optical axis of the SIT prototype. The prototype's optical axis is oriented strictly to the South at a 25° zenith angle (like all of the stations of the TAIGA-HiSCORE array). Single points far from the FOV's center of the SIT prototype in figure 12 (right) correspond to either very high energy events occurring near the SIT or to random coincidences within a given trigger mark window. This window will be tightened in further analysis when the all the delays in electronics will be properly evaluated.

Examples of events obtained by the SIT prototype detector are shown in figure 13. The color of pixels is proportional to the total charge collected in each SiPM near the trigger time.

2020 JINST 15 C09062

An example of one joint event is presented in figure 14 and figure 15. This event was detected on January 5th, 2020 in parallel by the SIT prototype detector and 13 HiSCORE stations. The image in figure 14 represents the signal integrals under peaks seen in figure 15 at time bin 98 in some pixels of the SIT prototype SiPM camera. The total signal over all SiPMs of the detector is around 200 photoelectrons. According to HiSCORE data the core of this event was located only 2 m away from the SIT detector and the arrival direction was near the optical axis of the prototype: the zenith angle is estimated to be $\theta = 24.53°$ and the azimuth angle $\phi = 358.33°$. The energy of this event is estimated as $2.3 \cdot 10^{17}$ eV.

6 Conclusions

In order to conduct long-term tests of the MicroFC-SMTPA-60035 SiPM and measuring system, the small imaging telescope (SIT) based on these SiPMs was installed in the Tunka Valley to work together with the TAIGA-HiSCORE array. The telescope's viewing angle was ±10°, the effective area of its entrance window was 0.1m^2. According to the TAIGA-HiSCORE array, it is possible to reconstruct the arrival direction, the position of the core and the energy of EAS. This allows to experimentally study the response of the SIT Cherenkov light flux from EAS with these characteristics. And also will allow the experimental study of the EASs' Cherenkov images in future SIT EASs' original parameters assessing with higher precision.

Acknowledgments

This work is supported by the Russian Science Foundation grant 19-72-20230.

References

[1] C. Baixeras et al., *Commissioning and first tests of the MAGIC telescope*, *Nucl. Instrum. Meth. A* **518** (2004) 188.

[2] C. Cortina et al., *Technical performance of the MAGIC telescope*, *Proc.* 29th *Int. Cosmic Ray Conf. Pune* **5** (2005) 359.

[3] T. Ashton et al., *A NECTAr-based upgrade for the Cherenkov cameras of the H.E.S.S.* 12*-meter telescopes*, *Astropart. Phys.* **118** (2020) 102425.

[4] CTA Consortium collaboration, *The Cherenkov Telescope Array*, in 16th *Rencontres du Vietnam. Theory meeting experiment: particle astrophysics and cosmology*, arXiv:2004.09213.

[5] CTA Consortium collaboration, *Introducing the CTA concept*, *Astropart. Phys.* **43** (2013) 3.

[6] L. Kuzmichev et al., *Cherenkov EAS arrays in the Tunka astrophysical center: from Tunka*-133 *to the TAIGA gamma and cosmic ray hybrid detector*, *Nucl. Instrum. Meth. A* **952** (2020) 161830.

[7] N. Budnev et al., *The TAIGA experiment: from cosmic-ray to gamma-ray astronomy in the Tunka valley*, *Nucl. Instrum. Meth. A* **845** (2017) 330.

[8] O. Gress et al., *The wide-aperture gamma-ray telescope TAIGA-HiSCORE in the Tunka valley: design, composition and commissioning*, *Nucl. Instrum. Meth. A* **845** (2017) 367.

[9] L.A. Kuzmichev et al., *TAIGA gamma observatory: status and prospects*, *Phys. Atom. Nucl.* **81** (2018) 497 [*Yad. Fiz.* **81** (2018) 469].

[10] D. Guberman and R. Paoletti, *Silicon photomultipliers in very high energy gamma-ray astrophysics*, 2020 *JINST* **15** C05039 [arXiv:2003.04086].

[11] MAGIC collaboration, *Performance of the MAGIC telescopes under moonlight*, *Astropart. Phys.* **94** (2017) 29 [arXiv:1704.00906].

[12] A. Biland et al., *Calibration and performance of the photon sensor response of FACT — the first G-APD Cherenkov telescope*, 2014 *JINST* **9** P10012.

[13] J. Aguilar et al., *Characterization and commissioning of the SST-1M camera for the Cherenkov Telescope Array*, *Nucl. Instrum. Meth. A* **845** (2017) 350.

[14] A. Asano et al., *Evaluation of silicon photomultipliers for dual-mirror small-sized telescopes of Cherenkov Telescope Array*, *Nucl. Instrum. Meth. A* **912** (2018) 177.

[15] A. Nagai et al., *Characterization of a large area silicon photomultiplier*, *Nucl. Instrum. Meth. A* **948** (2019) 162796.

[16] D. Impiombato et al., *Procedures for the relative calibration of the SiPM gain on ASTRI SST-2M camera*, *Exper. Astron.* **43** (2017) 1 [arXiv:1612.02186].

[17] S. Lombardi et al., *First detection of the Crab nebula at TeV energies with a Cherenkov telescope in a dual-mirror Schwarzschild-Couder configuration: the ASTRI-Horn telescope*, *Astron. Astrophys.* **634** (2020) A22 [arXiv:1909.12149].

[18] S.S. Zhang et al., *SiPM-based camera design and development for the image air Cherenkov telescope of LHAASO*, *Springer Proc. Phys.* **212** (2017) 17.

[19] B. Bi et al., *Performance of SiPMs and pre-amplifier for the wide field of view Cherenkov Telescope Array of LHAASO*, *Nucl. Instrum. Meth. A* **899** (2018) 94.

[20] A. Hahn et al., *Development of three silicon photomultiplier detector modules for the MAGIC telescopes for a performance comparison to PMTs*, *Nucl. Instrum. Meth. A* **912** (2018) 259.

[21] S. Ekoume et al., *A mini-imaging air Cherenkov telescope*, 2020 *JINST* **15** P04004.

[22] IceCube collaboration, *Design and performance of the first IceACT demonstrator at the South Pole*, 2020 *JINST* **15** T02002.

[23] *Oslo EDU* 6.6 *software webpage*, https://www.lambdares.com/edu/.

[24] *Xilinx Zynq-*7000 *SoC product webpage*, https://www.xilinx.com/products/silicon-devices/soc/zynq-7000.html.

[25] R. Antonov et al., *The SPHERE-*2 *detector for observation of extensive air showers in* 1 *PeV*–1 *EeV energy range*, *Astropart. Phys.* **121** (2020) 102460.

[26] R.A. Antonov et al., *Detection of reflected Cherenkov light from extensive air showers in the SPHERE experiment as a method of studying superhigh energy cosmic rays*, *Phys. Part. Nucl.* **46** (2015) 60.

2020 JINST 15 C09062